

COMPARATIVE STUDY WITH ALTERNATIVE MATERIALS FOR MANUFACTURE OF MACHINE TOOL STRUCTURES

Vitor Antonio Ducatti

Faculdade de Engenharia Civil, UNICAMP.
email: ducatti@fec.unicamp.br

Rosa Cristina Cecche Lintz

Faculdade de Engenharia Mecânica, UNICAMP
email: rosalintz@hotmail.com

José Maria C. Dos Santos

Faculdade de Engenharia Mecânica, UNICAMP
email: zema@fem.unicamp.br

Abstract. This paper presents a comparative study between static and dynamic test results achieved with some alternative materials used to manufacture machine tool structures. The part selected as a test prototype represents a lathe bed in actual scale. Based on this pattern twelve test prototypes were manufactured and the static and dynamic tests performed by using the following materials and/or composites: polymer mortar, polymer mortar with reinforcement cage, cast iron, cast steel, ferrocement with reinforcement cage, and fiber-reinforced mortar. Static tests were carried out to determine fatigue strength, bending stiffness, load-displacement curve under bending, and ultimate strength. Dynamic tests were made to obtain natural frequencies, damping rates, and mode shapes to the firsts deformed natural vibration modes. The results are compared and discussed in the aim to reveal the advantages and disadvantages in to use this alternative materials instead of the traditional ones, cast iron and cast steel, to manufacture machine tool structures.

Keywords. machine tool, reinforced ferrocement, polymer cement, fibrocement.

1. Introduction

Properties of high flexure and torsion static stiffness, good dynamic characteristics as high natural frequency and damping ratio, long-term dimensional stability, lower coefficient of thermal expansion and fabrication simplicity at low costs are required for machine tool structures. An important issue during the machining process is the chatter generated by self-excited vibrations. These vibrations can generate high levels of relative displacements between the part and the tool that compromise the accuracy of the final part. Such mechanism prevents higher cutting speeds and becomes an obstruction to reduce manufacturing times and costs. Traditionally, machine tool structures have been made by cast iron and cast steel, which can be cast into complex shapes, and easily machined to a high degree of accuracy. But, they also have some problems like high shrinkage rates during curing, long production lead-time, a need for special anti-corrosion treatment, high cost, etc.

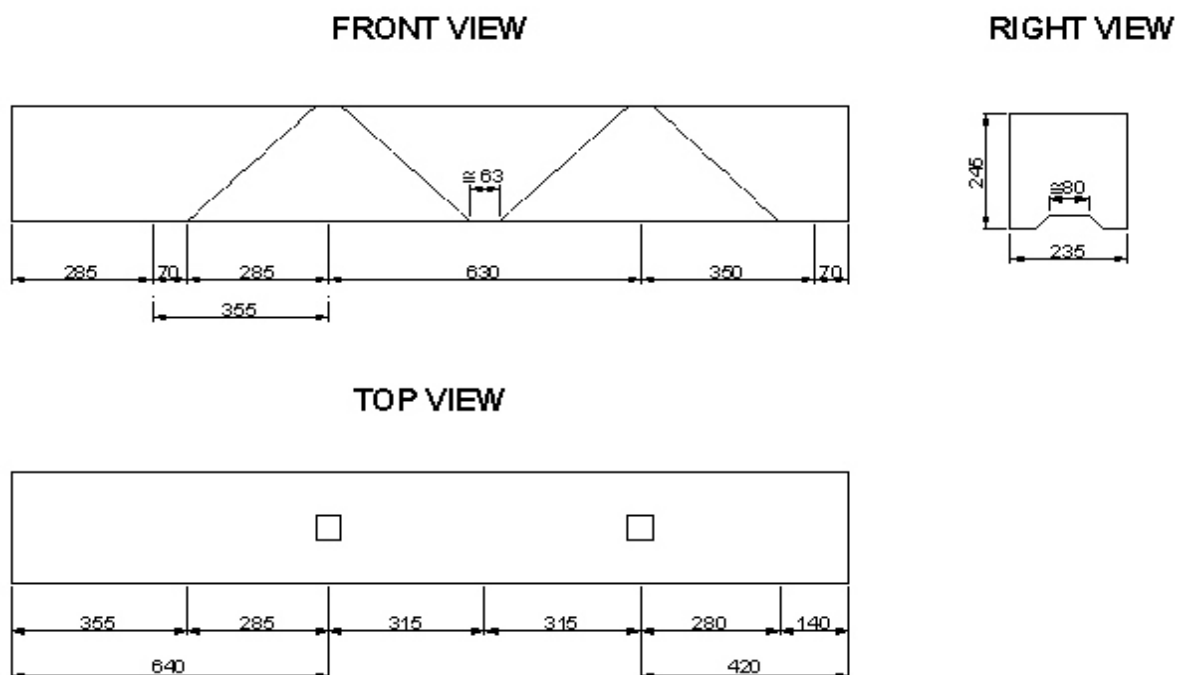


Figure 1. Geometry and main dimensions of the lathe bed prototype (units in mm).

Several attempts have been made either to supplement or to completely replace cast metals using mild steel weldments, synthetic granite, hydraulic cement concrete (ACI, 1989), polymer concrete (KANE, 1991; KOBLSICHEK, 1991), ferrocement (RAHMAN et al., 1987; RAHMAN et al, 1989), and fiber-reinforced concrete (RAHMAN & MANSUR, 1992).

This paper reports the effects to replace machine tools traditional materials by ferrocement, hydraulic cement mortar reinforced with steel fiber, polymer mortar, and reinforced polymer mortar. In this sense it presents a comparative study about the static and dynamic tests carried out with twelve prototype of a centre lathe bed (Figure 1).

2. Materials Properties and Prototypes Fabrication

Ferrocement, as the name implies, consists of iron or steel and cement. It is defined as type of thin wall reinforced concrete commonly constructed of hydraulic cement mortar reinforced with closely spaced layers of continuous and relatively small diameter wire mesh. The mesh may be made of metallic or other suitable material. Ferrocement differs from normal reinforced concrete because it uses wire mesh rather than heavy rods or bars, and uses sand rather than a mixture of sand and stone as the aggregate. Ferrocement utilized in this investigation is made up of high early strength portland cement (ASTM Type I), condensed silica fume, natural siliceous sand, and superplasticizer in the following proportion by weight: 1.00:0.20:2.00:0.26:0.02. Before mixing the ingredients, sand was passed through the 1.20 mm sieve. The fine wire mesh used in the reinforcement cages was of welded type with 12.5 mm square grids and 1.2 mm wire diameter, the yield strength of mesh reinforcement being 410 N/mm²

Fiber-reinforced mortar, is the ordinary concrete (mortar) containing discrete short length and small diameter fibers. The fibers are usually added to the concrete during mixing of its ingredients, and the resulting fiber concrete is directly poured into the mould simplifying the construction process considerably. The mix proportion of this mortar was the same of the ferrocement. Collated hooked-end steel fibers with aspect ratio 65 (35 mm long / 0.55 mm diameter) were incorporated to the mortar, in volume fractions of 1%, 2% and 3%, resulting in three distinct categories of resistance of fiber-reinforced mortar.

Polymer mortar, is the polymer composite utilized in this research was a mortar made up of three components: a liquid epoxy resin, a hardening agent, and a graded fine aggregate containing fine sand and filler. The mix proportion of aggregate and binder, by weight, was 6.75:1.00.

Reinforced polymer mortar, is the mortar with the same composition of polymer mortar which was reinforced with the same wire mesh (cage) of the ferrocement.

Cast iron, is a gray cast iron, GG 15 (lamellar graphitic) DIN 1691 with the following nominal average properties: 150 MPa tensile strength, 80 – 105 MPa yield strength, 550 – 700 MPa compression strength, 150 MPa shear strength, 230 – 370 bending strength, and 140 – 190 Brinell hardness.

Cast steel is a standard ASTM A 216 grade WCD.

Prototypes were named using the following abbreviations: AR1, AR2 and AR3 for the fiber-reinforced mortar with 1%, 2% and 3% volume fraction of fiber, respectively; AA for the ferrocement; AP for the polymer mortar; APA for the reinforced polymer mortar; FF for the cast iron; and AF for the cast steel. The mixes of portland cement mortar were made in one inclined axle intermittent concrete mixer. The batching procedure was as follows: (a) the cement and condensed silica fume pre-mixed was placed in the mixer; (b) then, half of the required water was mixed with a half of the superplasticizer and poured into the mixer; (c) these materials were mixed during three minutes; (d) the sand was added with the remaining water and superplasticizer; (e) with the mixer running, the fibers were sprinkled in by hand to assure even distribution. The total mixing period ranges from 10 to 15 minutes. The obtained mortars had presented consistency indexes of 253, 252, 223, and 210 mm, on the flow table, for the volume fiber of 0%, 1%, 2%, and 3%, respectively. These consistencies provided a ease consolidation of the mortar inside the moulds under the action of the vibratory table.

The total volume of polymer mortar needed for casting one prototype and the control specimens was separated in eight parts. Each of these parts was mixed in two stages. First, the sticky liquid phase, that is, the epoxy resin and the hardening agent were stirred with the help of a electric hammer drill with a shovel in the end. In the second stage, with the machine running, the aggregate mix was added bit by bit, and the mix continued until a homogenous colour of the material was reached. The polymer mortars were self-levelling and was moulded without vibration effort.

The mould to casting the cement mortar prototypes was made of fiber-glass (Figure 2) and for polymer mortar was made of wood. Figure 2a shows the mesh of reinforcement with the cage and Figure 2b shows the reinforcement with bars and stirrups. All prototypes includes a longitudinal reinforcement of four bars (10mm diameter), two for compression and two for tensile efforts. These bars were kept in position by three stirrups of 5 mm diameter.

3. Static Behavior

With the objective to determine deflection curves, static stiffness, first crack load and ultimate failure load, static tests were carried out (RAHMAN & MANSUR, 1992). The tests were made only to the cement mortar prototypes. The beds were simply supported as shown in Figure 3. Dial gauges were placed between underneath of the bed and a rigid support in order to measure its deflections. Concentrated forces were applied by an hydraulic jack at the points A, C and B, in this order, and the deflections computed.



Figure 2. Fiberglass mold: (a) reinforcement cage and (b) reinforcement bars & stirrups.

The load at the points A, C and B was carried out under the following instructions: a) the load was increased from 0 to 50 kN slowly and then reversed back at the same rate. The dial gauges were then initialised again; b) Load and deflection readings were taken at intervals of 5 kN up to the first crack appear (first crack load); c) After applying this procedure to the three points, the load-deflection curves and the ultimate bending load were obtained by loading only the central point B of the span.

Mechanical properties results of tested prototypes are presented in the Table 1. The results obtained for flexural tests with the prototypes made of mortars are presented in Table 2. The metal and polymer prototypes were not tested but their values for the stress and strain can be predicted through the equations of the classical strength of materials.

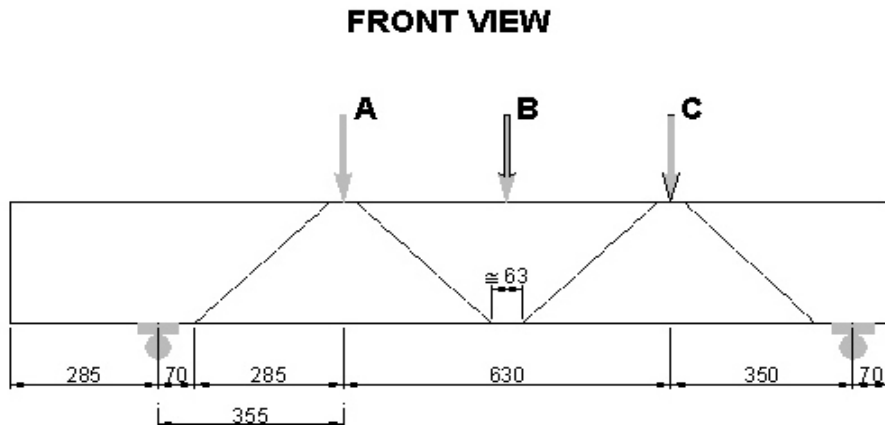


Figure 3. Applied constraints and loads diagram for the static tests (units in mm).

Table 1. Materials mechanical properties.

Mortar	Compressive Strength [MPa]	Tensile Strength [MPa]	Modulus of Rupture [MPa]	Elastic Modulus [GPa]
AR1	105	12	12	41
AR2	108	13	12	39
AR3	119	15	21	39
AA	103	7	11	41
AP	89	17	30	18

Table 2. First cracking and rupture loads.

Prototype	First cracking load [kN]			Rupture load [kN]
	A point	B point	C point	B point
AA	40	45	40	99
AR1	50	50	70	107
AR2	60	60	60	129
AR3	40	50	40	120

At the static tests one could be noticed the brittle failure of ferrocement and polymer mortar specimens, unlike of the gradually ductile failure of the fiber-reforced mortar. Due to addition of steel fibers the failure mode changed from a brittle failure to a fully ductile failure with a great increase in the post-crack energy absorption capacity. The first crack load did not changed with the increases of fibers percentage as it was expected, but the rupture load did. Figure 4a presents the load-deflection curves for the point B. Results confirm the increase in the flexural rigidity provided by the increasing fiber content. A comparison among the behavior of the prototypes shows that one made of ferrocement presents low ductility due the presence of wire mesh reinforcement, which results in a crushing failure. In the beds with fiber-reinforcement mortar the ductile behavior becomes evident from the rupture mode, where a characteristic noise at the instant before the failure was heard, which is originated from the fibers sliding inside of the matrix mortar. Fibers did not break, but were pulled out from the matrix. It was observed a plastic behavior among the models reinforced with fibers, resulting in a higher energy absorption capacity. The AR3 prototype had presented the highest toughness, represented by the area under the load-deflection curve, which confirms the literature results by RAHMAN & MANSUR (1992). These authors concluded that mortar beds with 3% volume fraction of fibers possess higher dimensional stability, strength and stiffness. At the end of static test it was noticed that the principal crack, in all beds, were bending cracks keeping their plane very close to the load action line. In the rupture of the beds with 2 and 3 % steel fiber was verified a little displacement of the principal crack related to the force application line. This behavior suggests that the more is the fiber content the more pronounced is this displacement. The amount of cracks at the instant of failure was observed, and it reveals that the fiber-reinforced beds have a larger number of cracks. The ferrocement bed presents failure through only one principal crack as the load increased up to happens a burst rupture.

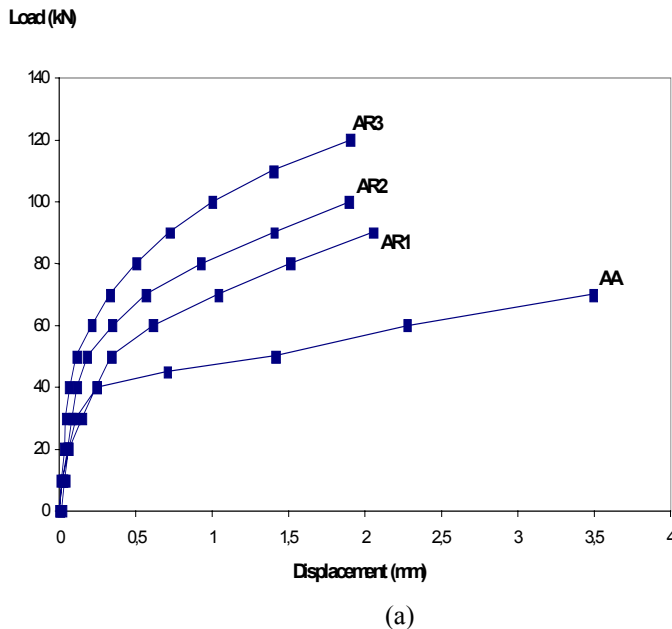


Figure 4. (a) Load x displacement plot measured and (b) Fatigue test experimental setup.

Fatigue tests were carried out with all mortar beds, obeying the same loading diagram (Figure 3) with the load at point B. Figure 4b shows the experimental set-up. The prototypes were subjected to a 150,000 cycles of repeated loading, at a frequency of 10Hz, prior to the static test to failure. The maximum load level of the cyclic load was 75% of first crack load and the minimum was 25%.

Table 3 shows the results of fatigue tests. The fifth column presents the results of the rupture in bending after the beds have been submitted to repeated load. The fourth column display these values for the beds that were not tested dynamically.

Table 3. Ultimate load before and after fatigue tests.

Prototype	Loading Amplitude [kN]		Bending Test before fatigue test [kN]	Bending Test after fatigue test [kN]
	min	max	Rupture load	Rupture load
AA	5	37,5	99	87
AR1	5	37,5	107	104
AR2	5	37,5	129	159
AR3	5	37,5	120	129
AP	8	60	-	150,90
APA	8	60	-	149,60

4. Dynamic Behavior

A technique commonly used to estimate dynamic system properties at low frequency ranges is the Experimental Modal Analysis (EMA). By using this technique 8 lathe beds were tested under free boundary conditions. The beds were mounted over pneumatics springs in order to obtain free boundary conditions at the experimental setup (Figure 5).



Figure 5. Dynamic experimental setup: (a) general view and (b) pneumatic springs detail.

Temperature variations during the test were neglected, because tests were made in acclimatized test room (constant environment temperature around 25°C). Lathe beds were forced in two directions transverse to the bed length through an electrodynamic shaker. The force was applied through a stinger connected to a piezoelectric force transducer, which was screwed to a metallic insert glued with epoxy at the bed surface (Figure 6a). A random noise signal was amplified and delivered to the shaker. For each excitation degree of freedom (vertical and horizontal) velocities of beds were measured at 54 points over the frequency range from DC-1024 Hz with a point laser Doppler vibrometer – LDV (Figure 6b). In order to improve the poor reflection of bed surfaces, and to localize measurement points in different tests, these

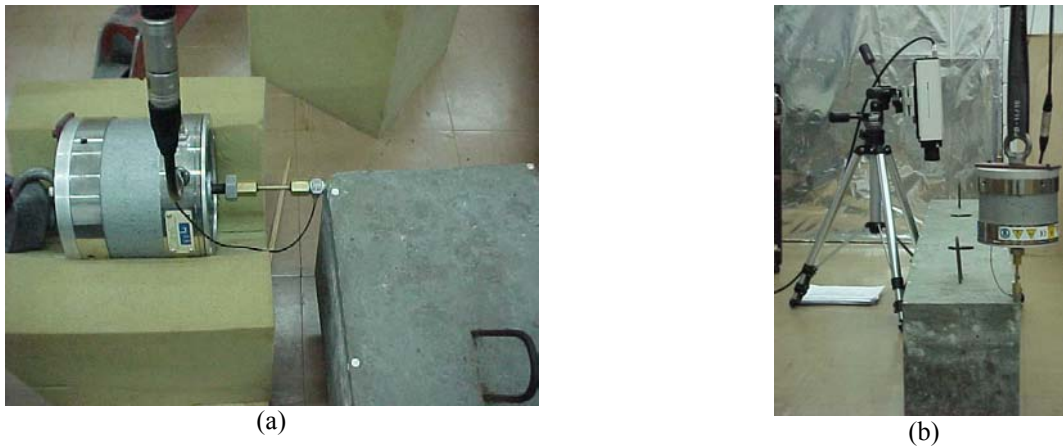


Figure 6. Excitation experimental setup: (a) horizontal excitation and (b) vertical excitation and velocity measurement.

were covered with small white paper stickers. The outputs of force transducer and LDV were sent to a data acquisition system (Hewlett Packard VXI-E1421B) and the signals processed in a modal analyses computational program (LMS-CADA-X3.5C).

The EMA procedure requires the definition of a measurement geometry, which includes all degrees of freedom measured and excited. From the lathe bed geometry, it was used a Cartesian coordinate system (X, Y, Z) with X along bed length and Y and Z in vertical and horizontal direction, respectively. Figure 7 shows the measurement points.

To the points 1 to 18 were taken velocity measurements in Y and Z directions, while to the points 19 to 36 were taken velocity measurements only in Z direction, and the velocities in Y direction were assumed as the same of point velocities for 1 to 18 in Y direction. It was possible due bed's mode dynamic symmetry. Although 54 point velocities have been measured, it was possible to carry out the modal analyses with 72 point velocities and 2 point forces (references), at point 9 directions $-Y$ and $+Z$. Frequency response functions (FRFs) were obtained with 1024 time samples, averaging over 30 blocks, using a Hanning window and frequency range DC-1024 Hz.

Modal parameter estimation was performed using the LMS-CADA-X[®] software with a time domain Polyreference Complex Exponential algorithm (VOLD, H., *et al.*, 1982). By utilizing simultaneously all FRFs, the method can extract natural frequencies, modal damping coefficients and vibration mode shapes for all modes in the frequency band that can be excited with the two references used. As a general rule, the 6 first deformable vibration modes were identified in a consistent way for the 8 lathe beds except to the fourth mode in the model FF. Table 4 and Table 5 shows the natural frequencies and modal damping coefficients identified, respectively.

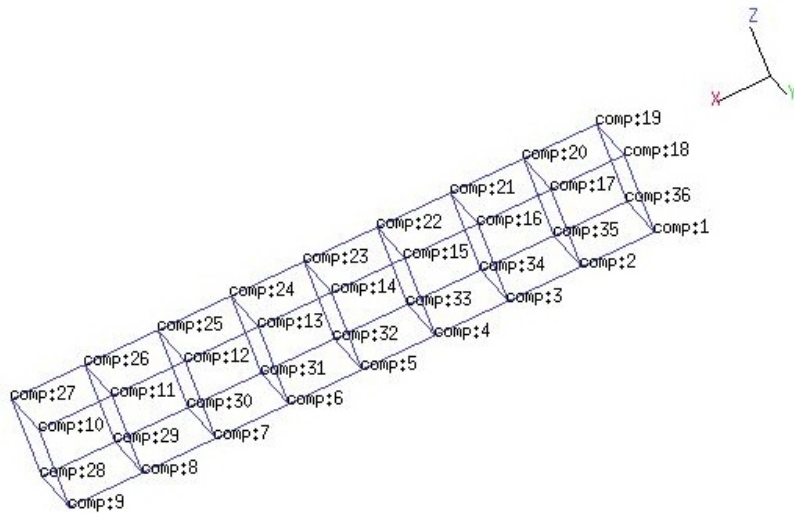


Figure 7. Measurement geometry configuration.

Table 4. Identified natural frequencies.

Mode	Natural frequency [Hz]							
	AF	FF	AR1	AR2	AR3	AA	AP	APA
1 – 1° Horizontal Bending	387.773	269.437	317.874	321.421	328.032	327.833	237.639	232.027
2 – 1° Vertical Bending	394.763	284.947	335.717	336.164	330.352	341.473	244.117	260.069
3 – 1° Torsion	599.917	401.887	407.440	387.603	409.480	474.453	279.510	314.434
4 – 2° Torsion	705.209	N/I*	494.578	509.744	508.098	516.131	339.472	412.347
5 – 2° Horizontal Bending	943.908	646.399	771.391	764.804	788.163	791.889	583.496	549.719
6 – 2° Vertical Bending	1011.390	711.305	820.512	840.944	854.801	870.658	628.169	625.531

* Not Identified

Table 5. Identified modal damping coefficients.

Mode	Modal damping coefficient [%]							
	AF	FF	AR1	AR2	AR3	AA	AP	APA
1 – 1° Horizontal Bending	0.344	0.458	0.706	0.457	0.517	0.586	0.526	0.511
2 – 1° Vertical Bending	0.216	2.239	1.568	0.714	0.376	1.997	0.526	2.900
3 – 1° Torsion	0.936	0.767	1.237	0.640	2.430	0.788	0.793	0.641
4 – 2° Torsion	0.687	N/I*	0.203	0.487	0.461	0.365	1.134	0.518
5 – 2° Horizontal Bending	0.140	0.583	0.775	0.502	1.377	0.426	0.848	0.778
6 – 2° Vertical Bending	0.751	0.183	1.189	0.733	0.653	0.778	0.717	0.642

* Not Identified

Plots in Figure 8 allow a better analysis of these results. Figure 8a shows that for the 6 first modes, as was expected, a clear predominance of the cast steel model (AF) at high natural frequencies could be noticed, followed by fiber-reinforced mortar (AR1/2/3) models, ferrocement model (AA), cast iron model (FF), and finally polymer cement models (AP and APA). This pattern could be verified in all modes except to the fiber-reinforced mortar models, where there were some inversions among different fiber percentage. Figure 8b shows a similar analysis to the modal damping coefficient. The cast steel model (AF) presents an expected behavior, i.e., the smaller damping to almost all analyzed modes, exception made to the mode 6.

However, for the other models it is noticed that damping coefficients presents huge variations from mode to mode. For mode 1 there is no significant variations between models, where all values are lower than 0.75% and model AR1 presents the higher damping coefficient. For mode 2 damping coefficient value for APA model is very high (2.9%) followed by FF, AA and AR1 models with values higher than 1.5%, which is much more higher than the others identified models. For mode 3 the AR3 model presents a damping coefficient value (2.43%) much more high than all the others. For modes 4, 5 and 6 there is predominance to the models AP, AR3 and AR1, respectively, all in the range from 1 to 1.5%, while the others present values inferior to 0.85%.

Based on this results it is difficult to get a precise criteria to choose a material that will introduce an effective structural damping, i.e., that ones with the major damping contribution to all identified modes. In order to improve the visualization of this contribution, and to minimize the bias introduced by the huge differences between the models in some modes, a median plot of modal damping coefficients was constructed (Figure 9). It is clear from this plot the AR1

model predominance followed by AP, AA, APA, AR3, AR2, FF e AF. This behavior corroborates some literature results (RAHMAN, M., *et al*, 1989; RAHMAN, M., & MANSUR, M. A., 1992; and KANE, J. F., 1991), which presents ferrocement, low fiber-reinforcement mortar, and polymer cement models with structural damping characteristics more effective than that obtained by traditional materials like cast iron and cast steel.

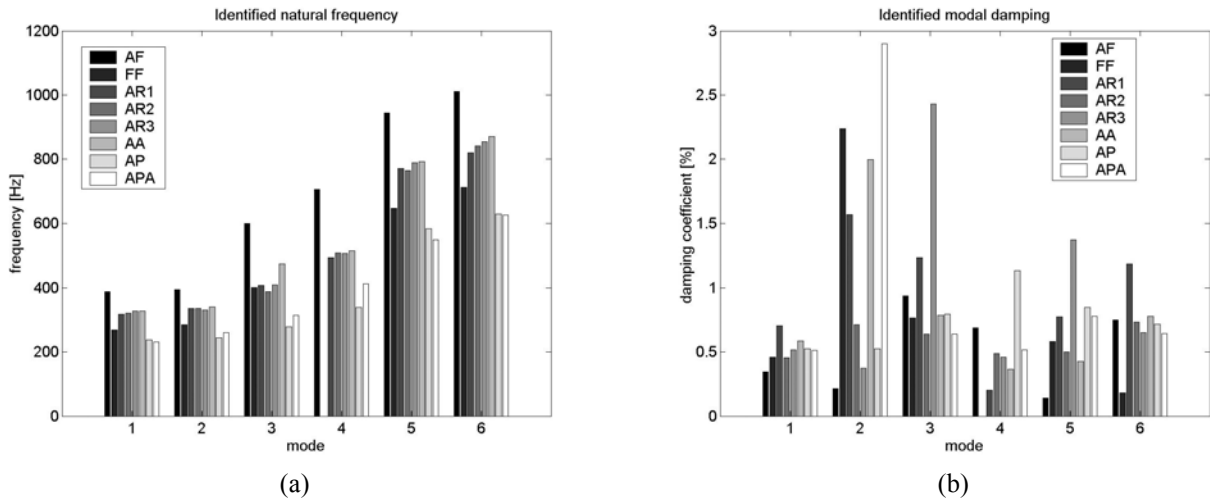


Figure 8. Identified results: (a) natural frequencies and (b) modal damping coefficients.

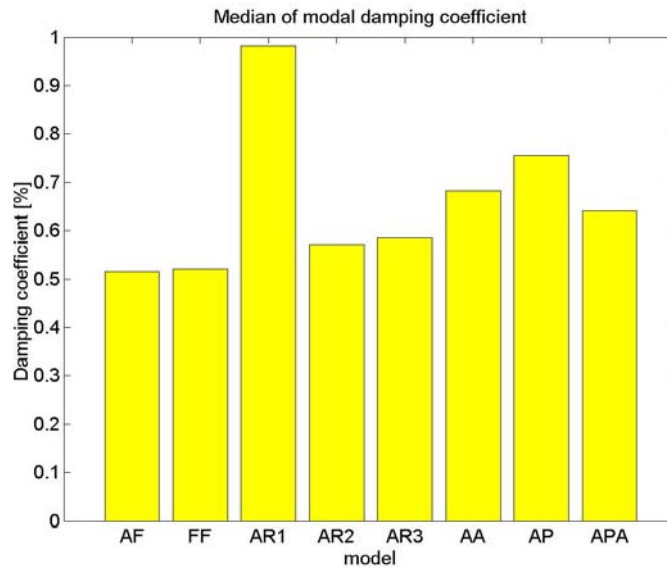
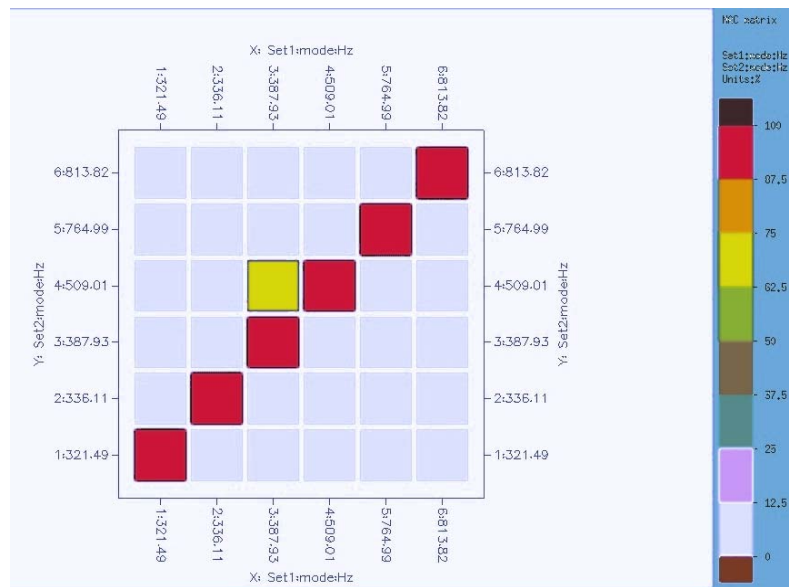


Figure 9. Median of modal damping coefficients.

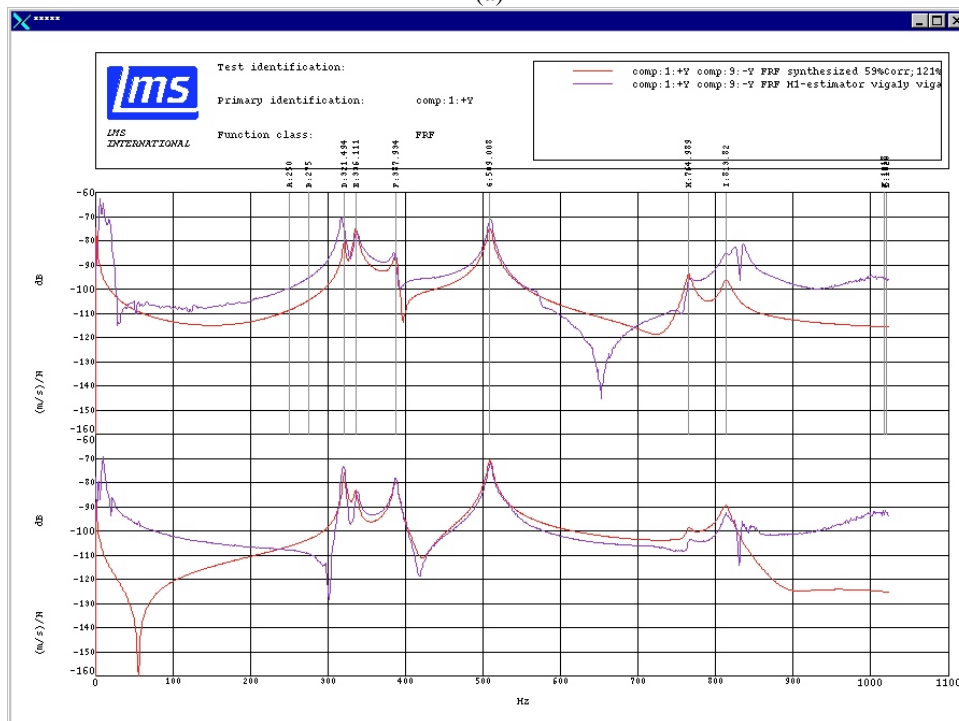
Although, Figure 9 plot demonstrate this tendency it is necessary to reevaluate the modal damping coefficients for each mode separately in a refined experimental modal analyses. It will increase the damping coefficient identification precision and hopefully will decreases the damping coefficient dispersion observed in some modes.

Figure 10a shows the modal assurance criteria (MAC) matrix and Figure 10b shows 2 different FRFs with measured and synthesized values to the lathe bed AR2. These results can be taken, at average, as a typical case, which represents that, occurred for all the other models and demonstrate the reliability of the identified experimental modes.

Figures 11 shows the identified mode shapes to 6 lathe beds (AF, AR3, AA, AP and APA). Models AR1 and AR2 were omitted since they do not presents significant differences related to the AR3 model.



(a)



(b)

Figure 10. Model AR2 identification readability: (a) modal assurance criteria matrix and (b) measured and synthesized FRFs.

5. Final Remarks

Twelve lathe bed prototypes in actual scale were fabricated with the following materials/composite: cast steel (AF); cast iron (FF); fiber-reinforced mortar (AR1, AR2 and AR3), ferrocement (AA); polymer mortar (AP); reinforced polymer mortar (APA). Static and dynamic tests were carried out on the beds and the results discussed with the aim to substitute the traditional materials, cast iron and cast steel, for the news ones, cement and polymer mortar. Static tests results in fiber-reinforced mortar beds show that first cracking loads range from 40 to 70 kN according to the load application point and fiber content included in the prototype. The maximum resulting displacements are lower than 5 mm. By assuming that the rupture happens in the beginning of the cracking, the fiber-reinforced mortar is able to support loads up to 40 kN. A lathe bed under service is not asked for such high loading. Therefore, as a static stiffness and strength of material point of view, the ferrocement and fiber-reinforced mortar prototypes are able to perform well as a machine tool lathe bed.

Rupture loads from prototypes loaded in the span center have no meaningful changes by comparing results from bending static test before and after cyclic loading. Only the AA prototype presents a rupture stress reduction of 14%,

while in the others this stress was kept unchanged. It reveals that cyclic loading seems to be no meaningful effect to the fiber-reinforced mortar prototypes. However, to the AP and APA prototypes the rupture loads were practically the same and very larger than (25%) that ones obtained with AR's prototypes after they have been submitted to cycle loading.

From the dynamic behavior, it is clear the experimental identification of the 6 first vibration modes for almost all prototypes. As expected, the cast steel dominance in terms of higher natural frequencies for all the modes demonstrate that the alternative materials will be the tendency to reduce them. Modal damping coefficients confirm some literature results related to alternative materials increase global damping when compared to the traditional ones. Of course, these are preliminary results and more research must be done in order to clarify the contributions to the damping coefficient rise for each mode separately.

6. Acknowledgment

The authors are grateful to LMS and Smartthec Companies for the free-use of CADA-X3.5C and to the government research agencies CNPq, CAPES, and FAPESP for the financial support.

7. References

- AMERICAN CONCRETE INSTITUTE. Manual of concrete practice: part 5. ACI. Measurement of properties of fiber reinforced concrete (ACI 544.2R-89). ACI Committee 544. Detroit, USA, 11p, 1989.
- AMERICAN SOCIETY FOR TESTING AND MATERIALS, ASTM C 78-94 . Standard Test Method for Flexural Strength of Concrete (using simple beam with third-point loading), Philadelphia, 3p, 1994.
- AMERICAN CONCRETE INSTITUTE. Polymer Concrete – Structural Applications State-of-the-Art Report (ACI 548.6R-96) ACI Committee 548, USA, 23p., 1996.
- AMERICAN CONCRETE INSTITUTE. Guide for the Use of Polymers in Concrete (ACI 548.1R-97) ACI Committee 548, USA, 29p, 1997.
- ASSOCIAÇÃO BRASILEIRA DE NORMAS TÉCNICAS (1984). NBR 08522- Concreto - Determinação do Módulo de Deformação Estático e Diagrama Tensão-Deformação - Método de Ensaio. Rio de Janeiro, 1984.
- ASSOCIAÇÃO BRASILEIRA DE NORMAS TÉCNICAS (1994). NBR 07222- Argamassa e Concreto - Determinação da Resistência à tração por compressão diametral de corpos de Prova Cilíndricos – Método de Ensaio. Rio de Janeiro, 1994.
- BS 1881: Part 116: 1983 - Method for determination of compressive strength of concrete cubes, 1983.
- KANE, J. F., Polymer Concrete Machine Tool Components, International 'Congress on Polymers in Concrete, North American Workshop, San Francisco, Sept. 1991.
- KOBLISCHEK, P.J. Polymer concrete as an alternative material for gray cast iron and welded steel construction in the machine tool industry. International Symposium on Brittle Matrix Composites, Frankfurt, pp 529-538, 1991.
- LMS CADA-X Version 3.5C (Software).
- NEVILLE, A. M. Propriedades do Concreto. PINI Editora, São Paulo, S.P., 1982.
- RAHMAN, M., *et al*, Design, fabrication and performance of a ferrocement machine tool bed, International Journal of Machine Tools and Manufacture, vol. 27, no. 4, pp. 431-442, 1987.
- RAHMAN, M., *et al*, A Study on the Application of Cementitious Materials for Machine Tools Structures, Bull. Japan Soc. Prec. Engg., vol. 23, No. 2, June, 1989.
- RAHMAN, M. & MANSUR, M. A.; Fiber reinforced concrete – A new material for machine tools. International Journal of Japan Society for Precision Engineering. Vol. 26(3), September, pp. 183-188, 1992.
- RAHMAN, M., *et al*, Development of a polymer impregnated concrete damping carriage for linear guide ways for machine tools, International Journal of Machine Tools and Manufacture, vol. 41, pp. 431-444, 2001.
- RAMAKRISHNAN, V.; BRANDSHAUG, T.; COYLE, W. V.; SCHRADER, E. K., A Comparative Evolution of Concrete Reinforced with straight Steel Fibers and Fibers with deformed ends Glued Together into Bundles. ACI Journal, Proceedings V. 77, n° 3, May-June, pp.135-143, 1980.
- RAMAKRISHNAN, V.; OBERLING, G.; TATNALL, P., Flexural Fatigue Strength of steel Fiber Reinforced Concrete. Fiber Reinforced Concrete-Properties and Applications, SP-105, American Concrete Institute, Detroit, pp.225-245, 1987.
- SOCIETY OF THE PLASTICS INDUSTRY, INC.. (SPI – 2.0). Test Methods for Compressive Strength of Cylindrical Polymer Concrete Specimens. Polymer Concrete Test Methods, New York, USA.
- SOCIETY OF THE PLASTICS INDUSTRY, INC.. (SPI – 5.0). Test Methods for Flexural Strength of Polymer Concrete (Using Simple Beam with Third-Point Loading). Polymer Concrete Test Methods, New York, USA.
- VOLD, H., *et al.*, A Multi-input Modal Parameter Estimation Algorithm for Mini-Computers, SAE paper 820194, 1982.

8. Copyright Notice

The authors are the only responsible for the printed material included in his paper.

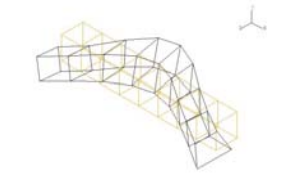
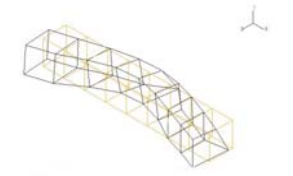
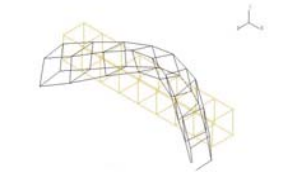
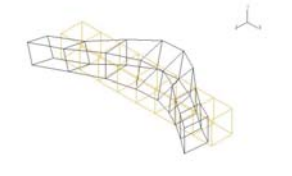
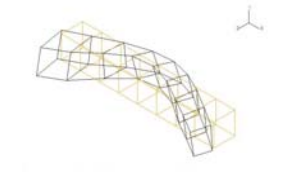
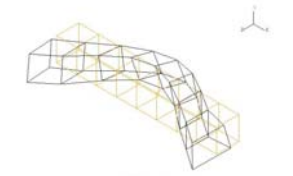
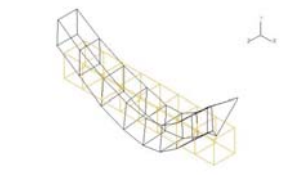
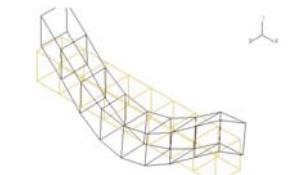

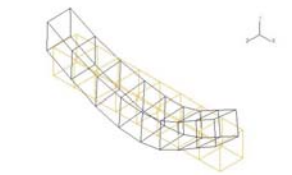
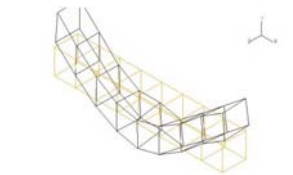
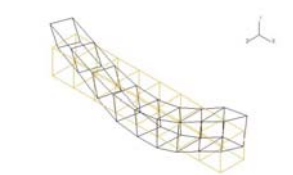
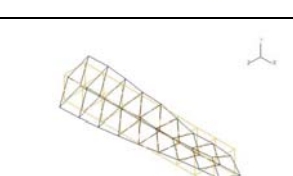
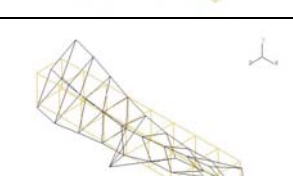
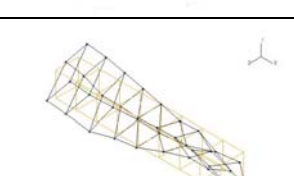
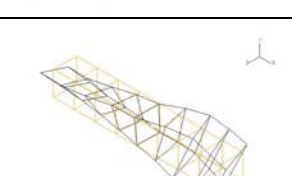

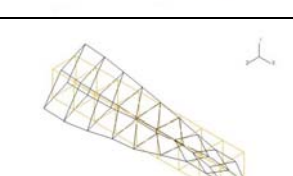
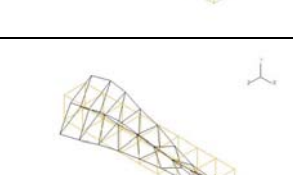
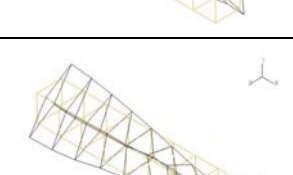
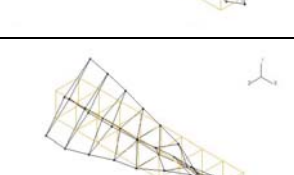
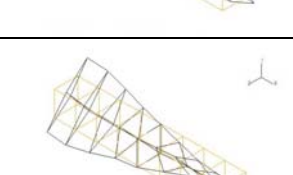
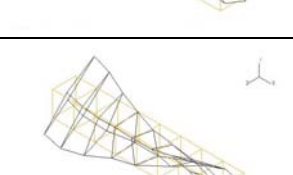
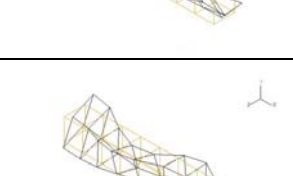

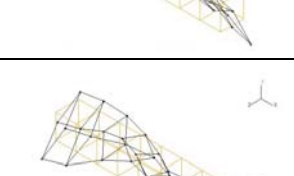
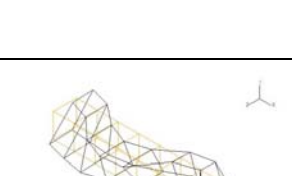
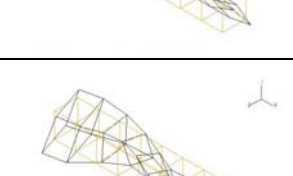
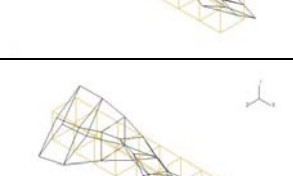
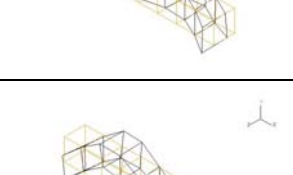
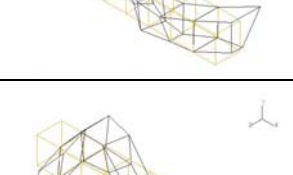

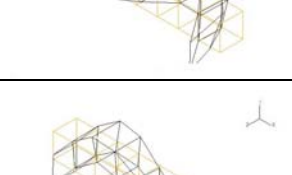
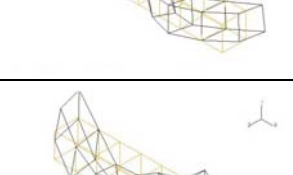
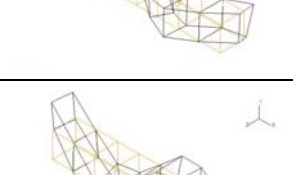
Mode	AF	AR3	AA	FF	AP	APA
1°. Horiz. Bending						
1°. Vertical Bending						
1°. Torsion						
2°. Torsion				Not Identified		
2°. Horiz. Bending						
2°. Vertical Bending						

Figure 11. Lathe beds vibration mode shape.